Universiteit Leiden
The Netherlands

Photochemical degradation pathways of cell-free antibiotic resistance genes in water under simulated sunlight irradiation: experimental and quantum chemical studies

Zhang, T.; Cheng, F.; Yang, H.; Zhu, B.; Li, C.; Zhang, Y.; ... ; Peijnenburg, W.J.G.M.

Citation
Zhang, T., Cheng, F., Yang, H., Zhu, B., Li, C., Zhang, Y., ... Peijnenburg, W. J. G. M. (2022). Photochemical degradation pathways of cell-free antibiotic resistance genes in water under simulated sunlight irradiation: experimental and quantum chemical studies. *Chemosphere*, *302*. doi:10.1016/j.chemosphere.2022.134879

Version:	Publisher's Version
License:	Licensed under Article 25fa Copyright Act/Law (Amendment Taverne)
Downloaded from:	https://hdl.handle.net/1887/3505217

Note: To cite this publication please use the final published version (if applicable).

Chemosphere 302 (2022) 134879

Contents lists available at ScienceDirect

Chemosphere

journal homepage: www.elsevier.com/locate/chemosphere

Photochemical degradation pathways of cell-free antibiotic resistance genes in water under simulated sunlight irradiation: Experimental and quantum chemical studies

Tingting Zhang [a], Fangyuan Cheng [a], Hao Yang [a], Boyi Zhu [a], Chao Li [a], Ya-nan Zhang [a,*], Jiao Qu [a,**], Willie J.G.M. Peijnenburg [b,c]

[a] State Environmental Protection Key Laboratory of Wetland Ecology and Vegetation Restoration, School of Environment, Northeast Normal University, Changchun, 130117, China
[b] Institute of Environmental Sciences, Leiden University, Leiden, the Netherlands
[c] National Institute of Public Health and the Environment (RIVM), Center for Safety of Substances and Products, Bilthoven, the Netherlands

HIGHLIGHTS

- Photodegradation of Tc-ARG was observed under simulated sunlight irradiation.
- Photodegradation of Tc-ARG was promoted by SRFA, and further inhibit its HGT.
- Mechanisms for the degradation and promotion of Tc-ARG were revealed by DFT.
- Tc-ARG can undergo fast photodegradation in the Yellow River estuary.

GRAPHICAL ABSTRACT

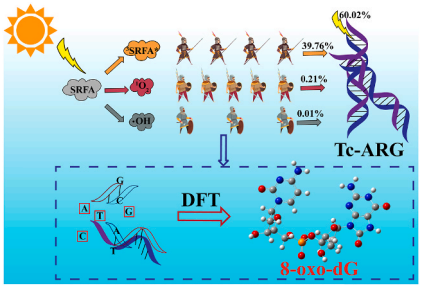

ARTICLE INFO

Handling Editor: Junfeng Niu

Keywords:
Antibiotic resistance genes
Photodegradation
Dissolved organic matter
Quantum chemical calculations

ABSTRACT

The presence of antibiotic resistance genes (ARGs) in the environment poses a threat to human health and therefore their environmental behavior needs to be studied urgently. A systematic study was conducted on the photodegradation pathways of the cell-free tetracycline resistance gene (Tc-ARG) under simulated sunlight irradiation. The results showed that Tc-ARG can undergo direct photodegradation, which significantly reduces its horizontal transfer efficiency. Suwannee River fulvic acid (SRFA) promoted the photodegradation of Tc-ARG and further inhibited its horizontal transfer by generating reactive intermediates. The photodegradation of Tc-ARG was attributed to degradation of the four bases (G, C, A, T) and the deoxyribose group. Quantum chemical calculations showed that the four bases could be oxidized by the hydroxyl radical (HO•) through addition and H-abstraction reactions. The main oxidative product 8-oxo-dG was detected. This product was generated through the addition reaction of G-C with HO•, subsequent to dissolved oxygen initiated H-abstraction and H_2O catalyzed H-transfer reactions. The predicted maximum photodegradation rates of Tc-ARG in the Yellow River estuary were 0.524, 0.937, and 0.336 h^{-1} in fresh water, estuary water, and seawater, respectively. This study

* Corresponding author.
** Corresponding author.
E-mail addresses: zhangyn912@nenu.edu.cn (Y.-n. Zhang), quj100@nenu.edu.cn (J. Qu).

https://doi.org/10.1016/j.chemosphere.2022.134879
Received 24 March 2022; Received in revised form 29 April 2022; Accepted 5 May 2022
Available online 10 May 2022
0045-6535/© 2022 Elsevier Ltd. All rights reserved.

furthermore revealed the microscopic photodegradation pathways and obtained essential degradation parameters of Tc-ARG in sunlit surface water.

1. Introduction

Antibiotic resistance genes (ARGs) represent a kind of emerging pollutants (Pruden et al., 2006) which pose a serious threat to human health and the ecosystem (Luo and Zhou, 2008). ARGs are ubiquitous in the environment and have been detected in water bodies, soils, sediments, and other environmental media (Zhang et al., 2018a). Among these media, water bodies were proven to be a main reservoir of ARGs. Distinct from traditional pollutants, ARGs could spread through two pathways: vertical gene transfer (VGT) and horizontal gene transfer (HGT) (Alekshun and Levy, 2007; Chen et al., 2015). HGT is realized through transformation, transduction, and combination mechanisms (Chen et al., 2019).

In natural waters, ARGs mainly exist in two forms: the genes in cells, i.e. intracellular ARGs (i-ARGs) and the genes directly exposed in the environment, i.e. extracellular ARGs (e-ARGs) (Chang et al., 2017). The i-ARGs mainly transfer via transduction by bacteriophages and by combination with mobile genetic elements (MGEs), such as plasmids, transposons, and integrons, from one bacteria to another bacteria, while e-ARGs mainly spread through transformation into bacteria. The latter occurs more frequently in the aquatic environment and among the detected e-ARGs, tetracycline and sulfonamide are the most common resistance genes (Qiao et al., 2018). Especially plasmid-mediated transformation has been extensively investigated (Bellanger et al., 2014; Dang et al., 2017; Zhao et al., 2020). The spread of ARGs in water can increase their exposure risks to human beings (Luo and Zhou, 2008; Amarasiri et al., 2020). Therefore, it is of great significance to investigate the transformation behavior of e-ARGs in natural waters.

It is well known that photochemical transformation induced by sunlight is the main degradation pathway of emerging organic pollutants in surface water (De Hoe et al., 2019; Edhlund et al., 2006; Li et al., 2016). Previous studies have also shown that light irradiation can induce degradation of ARGs (Zhang et al., 2019a), and ultraviolet disinfection can also reduce e-ARGs to a certain extent (Zhang et al., 2019b; McKinney and Pruden, 2012; Sinha and Hader, 2002). For example, Chang et al. (2017) reported that e-ARGs can be degraded under UV_{254}. Apart from this, efficient degradation of ARGs can occur under the action of UVB (290–380 nm) (Cheng et al., 2022) and slight degradation can occur under UVA (300–400 nm) irradiation (Moreira et al., 2018). Recently, it was shown that ARGs can undergo direct photodegradation under simulated sunlight irradiation (Zhang et al., 2020a).

Besides direct photodegradation, ARGs can also undergo dissolved organic matter (DOM) induced indirect photodegradation. In previous studies, ARGs were proven to be efficiently degraded in the UV/H_2O_2 and UV/chlorine systems, as mainly induced by generated reactive species, especially hydroxyl radicals ($HO^{\bullet}$) (Wang et al., 2020; Yoon et al., 2017; Phattarapattamawong et al., 2021). In sunlit surface water, photochemically produced reactive intermediates (PPRIs), such as $HO^{\bullet}$ and singlet oxygen ($^1O_2$) can be generated, and DOM is an important sensitizer that induces the generation of these PPRIs (Wang and Chen, 2020; Wenk et al., 2011). Zhang et al. (2019a) found that the presence of DOM could promote the photodegradation of *tet*A and bla_{TEM-1} resistance genes due to the generation of $HO^{\bullet}$ and $^1O_2$, and the promotional effect of DOM on the photodegradation of ARGs further inhibited its transformation rate. $^1O_2$ could result in the damage of bases in DNA molecules through oxidation (Ravanat et al., 2001; Zhang et al., 2019a). However, the detailed photodegradation pathways of ARGs at the molecular level are still not fully understood.

ARG is a DNA fragment with a special expression function, and the basic unit of DNA is deoxyribonucleosides (dG, dC, dT, dA) which consist of four bases (G, C, T, A) and deoxyribose. The photodegradation of e-ARGs under sunlight irradiation may mainly be attributed to the degradation of the four deoxyribonucleosides or bases. Therefore, the photodegradation pathways of deoxyribonucleosides and bases, especially their detailed reactions with reactive species, need to be revealed. Density functional theory (DFT) calculations are regarded as an efficient tool to probe reaction mechanisms, and have been frequently used to investigate the reaction pathways of organic pollutants with reactive species (Li et al., 2014; Fu et al., 2016). The reactions pathways of organic pollutants with $HO^{\bullet}$, chlorine radicals, and superoxide radical have been well investigated using DFT calculation, of which results is in according with the experimental results (Bai et al., 2022; Li et al., 2014; Luo et al., 2021; Zhang et al., 2018b).

Thus in this study, the photodegradation of ARGs was investigated with the tetracycline resistance gene (Tc-ARG) as a representative. Tc-ARG was selected due to its ubiquity in the aqueous environment with concentrations ranging from 10^1-10^6 copies mL^{-1} (Jiang et al., 2013; Qiao et al., 2018). The pBR322 plasmid that is carrying Tc-ARG, was selected as the target plasmid. The effect of DOM was studied with Suwannee River fulvic acid (SRFA) as a representative. To elucidate the degradation pathways of Tc-ARG, photodegradation of the four deoxyribonucleosides and bases were investigated and the detailed reaction pathways of the four bases with typical reactive intermediate were calculated with DFT. The photolysis rate constant of Tc-ARG in natural waters was also predicted. The study provides basic data and the scientific basis for revealing the migration and transformation behavior of ARGs in natural waters.

2. Materials and methods

2.1. Materials

pBR322 plasmid (0.5 g L^{-1}, 4361 bp, NCBI GenBank NO. J01749.1) that is carrying the tetracycline resistance gene (Tc-ARG, *tet*A, 1261 bp) was purchased from ThermoFisher Scientic Inc. The plasmid was used as representative e-ARGs, and the sequences of the target gene and primer are listed in Table S1 in the Supporting Information (SI). Suwannee River fulvic acid (SRFA, 2S1010F) was purchased from the International Humic Substances Society. *E.coli* HB101 competent cells that were purchased from the Takara Biotechnology Co. Ltd. (Dalian, China) were used as recipient bacteria. Deoxyribonuclease I (DNase I), phosphodiesterase I, alkaline phosphatase (ALPase), deoxyguanosine (dG), deoxyadenosine (dA), and deoxythymidine (dT) were obtained from Sangon Biotech Co. Ltd. (Shanghai, China). Deferoxamine mesylate (DFO), 8-hydroxy-2′-deoxyguanosine (8-oxo-dG), deoxycytidine (dC), rose bengal (RB), furfuryl alcohol (FFA, 98%), sorbic acid (SA, 99%), acetophenone (AP, 98%), benzene (98%), phenol and 2,4,6-trimethylphenol (TMP, 99%) were purchased from J&K Scientific. All other chemicals, materials, and corresponding commodity suppliers are listed in Test S1 in the SI.

2.2. Steady-state irradiation experiments

The steady-state irradiation experiments were carried out in an XPA-7 merry-go-round photochemical reactor (Xujiang Electromechanical Plant, Nanjing, China) with quartz tubes containing the Tc-ARG sample. A water-cooled 1000 W Xenon lamp equipped with 290 nm filters was used to imitate the sunlight. The light intensity at the surface of the quartz tube was detected with a TriOS-RAMSES spectroradiometer (TriOS GmbH, Germany), and the results are shown in Fig.S1. In the irradiation experiment, the stirring speed of the DNA sample was

controlled at 300 ± 5 rpm, and the condensate temperature was controlled at 25 ± 1 °C using the condensing device.

The plasmid was dissolved in phosphate buffer solution (PBS) to ensure that the pH = 7.0 and some quartz tubes wrapped with two layers of aluminum foil were used as dark controls. The volume of the plasmid solution is 4.0 mL and the initial concentration was 1 μg mL^{-1}. At different intervals (0, 30, 60, 90, 120, 240 min), 100 μL sample were taken from a tube, and Tc-ARG was determined by real time-quantitative polymerase chain reaction (RT-qPCR) with short primer. The detailed methods are given in the SI (Text S2).

To explore the effect of DOM, SRFA was added with an initial concentration of 10 mg L^{-1} (4.8 mgC L^{-1}). The concentration of SRFA was selected to be consistent with the concentration of DOM in surface water (Zhang et al., 2018b). The role of PPRIs produced by SRFA was explored by performing quenching experiments. IPA (25 mM) was used as a scavenger to remove HO• (Latch et al., 2003), FFA (1 mM) to remove $^1O_2$ (Fan et al., 2019), and SA (2 mM) to remove excited triplet state of SRFA (^{3}SRFA*) (Grebel et al., 2011). The steady-state concentration of the PPRIs, including ^{3}SRFA*, $^1O_2$, and HO•, were determined using chemical probes such as 2,4,6-trimethylphenol for ^{3}SRFA*, FFA for $^1O_2$, and benzene for HO• (Zhou et al., 2018).

The basic units of DNA are the four bases. To further clarify the degradation pathway of ARGs, the photochemical degradation kinetics of the four bases were measured, and a two-base DNA strand (G-C) was used as a representative to investigate the photodegradation of short-stranded DNA. The steady-state irradiation experiments were the same as performed for Tc-ARG as described above, and the quantitative analysis method of the bases and G-C is described in Text S3 in the SI.

2.3. Transformation experiments

The transformation experiments were performed to study the change of the HGT ability of e-ARGs during the photodegradation. The degraded plasmid was purified by purification kits and then transferred into 50 μL E.*coli* HB101 solutions. The transformed bacteria were spread on the culture medium (tetracycline-resistant bacteria and total bacteria were counted in selective medium and normal medium, respectively.), and subsequently cultured at a constant temperature of 37 °C for 24 h. The colony-forming units (CFU) were counted manually. The detailed method of the transformation experiments is shown in Text S4.

Transformation efficiency was calculated according to equation eq. (1):

$$\text{transformation efficiency} = \frac{\text{transformed CFU}}{\text{total CFU}} \tag{1}$$

where the transformed CFU represented the colony number on solid medium with tetracycline and the total CFU was on medium without tetracycline.

2.4. Determination of second-order reaction rate constants of Tc-ARG with PPRIs

The second-order reaction rate constants of Tc-ARG with PPRIs are essential to assess the elimination rate in natural waters induced by sunlight. Thus, the second-order reaction rate constants between Tc-ARG and ^{3}SRFA*, $^1O_2$, HO• were determined. The detailed methods for determining the second-order reaction rate constants between Tc-ARG and $^1O_2$, HO• are described in Text S5 and S6, and they are shown below for the reaction of Tc-ARG with ^{3}SRFA*.

The photolysis rate constant ($k_{obs\ (SRFA)}$) of Tc-ARG in the presence of SRFA is composed of direct photodegradation ($S_\lambda k_d$) and indirect photodegradation (k_{ind}) as shown in eq. (2):

$$k_{obs(SRFA)} = S_\lambda k_d + k_{ind} \tag{2}$$

where S_λ is the sum of the light screening factors of SRFA that could be calculated by eqs. (3)–(5) (Zhang et al., 2018b), k_d is the direct photodegradation rate constant; k_{ind} can be calculated using eq. (2).

$$S_\lambda = \frac{1 - 10^{-(\alpha_\lambda l + \varepsilon_\lambda [ARG]) l}}{2.303(\alpha_\lambda + \varepsilon_\lambda [ARG]) l} \tag{3}$$

$$l = \frac{\pi r^2}{2r} \tag{4}$$

$$\sum S_\lambda = \frac{\sum I_\lambda S_\lambda \varepsilon_\lambda}{\sum I_\lambda \varepsilon_\lambda} \tag{5}$$

where α_λ is the light attenuation coefficient of SRFA at λ (cm^{-1}), measured by a UV–Vis spectrophotometer (Hitachi U2900); ε_λ is the molecular absorption coefficient (cm^{-1} L^{-1} mol); l is the length of the light path of the quartz photolysis tube (cm); r is the inner radius of the quartz photolysis tube, 0.65 cm was used here; I_λ is the Incident light intensity (Einstein s^{-1} cm^{-2}).

$$\begin{aligned} k_{ind} &= k_{1O2} + k_{HO\cdot} + k_{3SRFA^*} \\ &= k_{ARGs,1O2}\left[{}^1O_2\right]_{SS} + k_{ARGs,HO\cdot}[HO\cdot]_{SS} + k_{ARGs,3SRFA^*}\left[{}^3SRFA^*\right]_{SS} \end{aligned} \tag{6}$$

$$\begin{aligned} k_{ARGs,3SRFA^*} &= \frac{k_{3SRFA^*}}{[{}^3SRFA^*]_{SS}} = \frac{k_{ind} - k_{1O2} - k_{HO\cdot}}{[{}^3SRFA^*]_{SS}} \\ &= \frac{k_{ind} - k_{ARGs,1O2}[O_{21}]_{SS} - k_{ARGs,HO\cdot}[HO\cdot]_{SS}}{[{}^3SRFA^*]_{SS}} \end{aligned} \tag{7}$$

where $k_{ARGs,1O2}$, $k_{ARGs,HO•}$ and $k_{ARGs,3SRFA*}$ are the second-order reaction rate constants of e-ARGs with $^1O_2$, HO• and ^{3}SRFA*, among which $k_{ARGs,1O2}$ and $k_{ARGs,HO•}$ being determined by competitive dynamics (Text S5 and S6). The steady concentration of PPRIs generated by SRFA, containing $[^1O_2]_{SS}$, $[HO•]_{SS}$ and $[^3SRFA*]_{SS}$ was obtained with the methods described in Text S7 in the SI, $k_{ARGs,3SRFA*}$ could be calculated using eq. (7).

2.5. Degradation kinetics of deoxyribonucleosides and detection of 8-oxo-dG

The degraded pBR322 plasmid (100 μL), of which the initial concentration was 10 μg mL^{-1}, was purified using DNA purification kits. Thereafter, 1.0 U DNase I, 0.1 U phosphodiesterase I, and 1.0 U ALPase were added for the digestion of the pBR322 plasmid, and DFO (1 mM) was added to prevent the oxidation of the DNA. The solutions were subsequently put in the dark at 37 °C for 24 h. The digested samples were analyzed using high-performance liquid chromatography (HPLC) to detect the concentrations of deoxyguanosine (dG), deoxycytidine (dC), deoxyadenosine (dA), and deoxythymidine (dT). High-performance liquid chromatography coupled with mass spectrometry (HPLC-MS) was used to determine the oxidation products (8-oxo-dG). The detailed analysis methods are described in Text S8 in the SI.

2.6. DFT calculations

To elucidate the microscopic photodegradation pathways of Tc-ARG, the reaction pathways of the four DNA bases and the two-base DNA (G-C as an example) with HO• were calculated with DFT. All DFT calculations were performed using the Gaussian 16 software package (Frisch et al., 2016). Previous studies have shown that the B3LYP function is credible (Li et al., 2014; Zhang et al., 2019c), so optimization and vibration frequency analysis were performed at the B3LYP/6–31++G (d, p) level. The integral equation formalism of the polarized continuum model (IEFPCM) using the self-consistent reaction field method was used to consider the solvent effect of water. Transition states (TS) were verified by the only imaginary vibrational frequency and intrinsic reaction coordinate (IRC) analysis (Fukui, 1981). Single-point energy calculation was performed at the B3LYP/6–311++G (3df, 2p) level, and zero-point

correction was performed to obtain the thermodynamic energies (Gibbs energy and enthalpy).

3. Results and discussion

3.1. Photodegradation of Tc-ARG and influence of SRFA

Tc-ARG could be directly degraded under simulated sunlight irradiation, and no obvious degradation was observed under dark conditions (Fig. 1(a)). Therefore, light irradiation is the main force for the degradation of Tc-ARG. The photodegradation of Tc-ARG followed pseudo-first-order kinetics and the observed photolysis rate constant (k_{obs}) was calculated to be 1.74 ± 0.02 h^{-1}. The apparent quantum yield (Φ) of Tc-ARG was calculated to be 1.56 ± 0.12 with the method detailed in Text S9.

In RB solution (10 μM), the k_{obs} of Tc-ARG was 2.17 ± 0.07 h^{-1} under simulated sunlight irradiation that is higher compared with the k_{obs} in PBS. This indicated that $^1O_2$ is capable of initiating the degradation of Tc-ARG. In H_2O_2 solution (20 mM), the degradation rate was accelerated up to a value of 3.06 ± 0.03 h^{-1}. This indicates that HO• could also oxidize Tc-ARG. Thus, the second order reaction rate constants of Tc-ARG with $^1O_2$ ($k_{ARGs,1O2}$) and HO• ($k_{ARGs,HO•}$) were determined, and the values are (8.44 ± 0.12) × 10^6 M^{-1} s^{-1} and (5.11 ± 0.11) × 10^{10} M^{-1} s^{-1}, respectively.

In SRFA solutions, the k_{obs} was 2.58 ± 0.05 h^{-1}, which is higher compared with that in PBS. This indicates that SRFA can promote the photodegradation of Tc-ARG. The promotional effect of Suwannee River natural organic matter (SRNOM) on the photodegradation of e-ARGs was also observed in a previous study (Zhang et al., 2019a).

Cell-free ARGs are considered to be a neglected source for ARGs spreading in wastewater treatment plants (Zhang et al., 2018a), of which the effluent will be discharged into natural waters and induce the HGT of ARGs subsequently. Thus, the horizontal transformation efficiency of Tc-ARG during its photodegradation was determined, and the results are shown in Fig. 1(b) and Table S2 in the SI. As can be seen in Fig. 1(b), the transformation efficiency of Tc-ARG was significantly suppressed, and as the irradiation time increased, the inhibitory effect was enhanced.

In the RB and H_2O_2 solutions, the transformation efficiencies of Tc-ARG were also decreased under simulated sunlight irradiation, implying that $^1O_2$ and HO• initiated reactions can also inhibit the HGT of Tc-ARG. Thus, the generated reactive oxygen species (ROSs) could play a role in the elimination and spread of cell-free ARGs. In the presence of SRFA, the transformation efficiency was also significantly inhibited under simulated sunlight irradiation, and the inhibitory effect is stronger compared with that in PBS. Therefore, it can be concluded that the photodegradation of Tc-ARG in surface water could lead to the decline of HGT capacity, thereby inhibiting the diffusion of ARGs in natural waters.

3.2. Contribution of PPRIs to Tc-ARG photodegradation

As shown above, SRFA can promote the photodegradation of Tc-ARG and inhibit its HGT. As reported in previous studies, SRFA promoted the photodegradation of organic pollutants through the generation of PPRIs, including ^{3}SRFA*, $^1O_2$, and HO• (Leresche et al., 2016; Guo and Jans, 2006; Chin et al., 2004). Therefore, the mechanism causing the impact of SRFA on the photodegradation of Tc-ARG was further explored by quenching experiments (see in Fig. 2). Addition of IPA and FFA was found to significantly inhibit the photodegradation of Tc-ARG. This indicates that $^1O_2$ and HO• involved in SRFA initiated indirect photodegradation of Tc-ARG. The addition of SA also significantly decreased the k_{obs} of Tc-ARG. The inhibitory effect of SA is thus much stronger as compared to IPA and FFA. Thus, ^{3}SRFA* played a more important role in the indirect photodegradation of Tc-ARG induced by SRFA.

To calculate the contribution rate of PPRIs, steady-state concentrations of the PPRIs in the SRFA solution were calculated, and the results are shown in Table S3. The $k_{ARGs,3SRFA*}$ was calculated with eq. (6) and the value is 3.65 × 10^9 M^{-1} s^{-1}. Based on the calculated reaction rate constants and the concentrations of the PPRIs (Table S3 and S4), contribution rates of direct photodegradation, $^1O_2$, HO•, and ^{3}SRFA* to the photodegradation of Tc-ARG were calculated to be 60.02, 0.21, 0.01, and 39.76%, respectively with the method detailed in Text S10. It is consistent with the results of the quenching experiments that besides direct photodegradation, the contribution of ^{3}SRFA* is the largest. These results differ from the experimental results reported by Zhang et al. (2019a). These authors attributed the SRNOM induced indirect photodegradation of e-ARGs mainly to $^1O_2$ and HO•, which reflects the different influence mechanisms of SRFA and SRNOM on the photodegradation of e-ARGs.

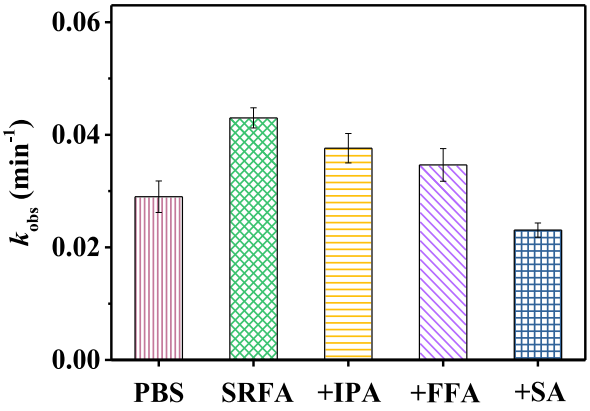

Fig. 2. Pseudo first order kinetic constants of Tc-ARG (C_0 = 1 μg mL^{-1}) in PBS and in SRFA solutions (10 mg L^{-1}) with different quenchers (IPA: 25 mM; FFA: 1 mM; SA: 2 mM pH = 7.0).

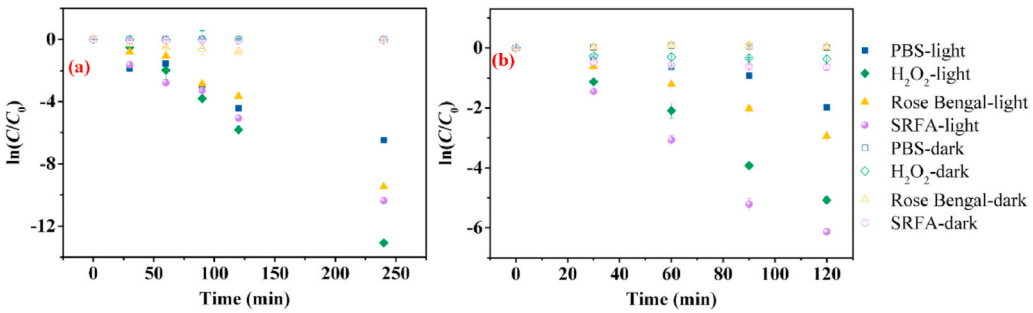

Fig. 1. Photodegradation kinetics of Tc-ARG in different solutions (C_0 = 1 μg mL^{-1}) **(a)** and changes in transformation efficiencies **(b)** at pH = 7.0.

3.3. Degradation of deoxynucleosides and generation of 8-oxo-dG during photodegradation of e-ARGs

The main pathways of DNA damage are strand breaks and base damage (Zhang et al., 2019a; Yoon et al., 2017). Therefore, to further understand the photodegradation pathways of e-ARGs, the changes in the concentration of the four deoxynucleosides (dG, dC, dA and dT) during the photodegradation of Tc-ARG were investigated. The degradation kinetics of the four deoxynucleosides were obtained by digesting Tc-ARG during its photodegradation and detecting their concentrations using HPLC. The results showed that all four deoxyguanosines could undergo degradation during the photodegradation of Tc-ARG under direct light irradiation, and none of the deoxynucleosides degraded under dark conditions (Fig. 3). The values of k_{obs} of dG, dC, dA and dT were calculated to be 0.0011 ± 0.0001, 0.0048 ± 0.0001, 0.0016 ± 0.0001 and 0.0107 ± 0.0010 h^{-1}, respectively (Table S5). These results demonstrated that sunlight irradiation could induce photodamage of deoxynucleosides in e-ARGs. The results are consistent with the research findings of Zhang et al. (2020b).

The presence of SRFA could promote the degradation of the four deoxynucleosides, where the values of k_{obs} of dG, dC, dA and dT were 0.0047 ± 0.0001, 0.0061 ± 0.0003, 0.0020 ± 0.0001 and 0.0123 ± 0.0012 h^{-1}. They were thus increased by 327, 27, 25 and 15% respectively compared with the raters determined in PBS. Among the four deoxynucleosides, SRFA exhibited the greatest role in promoting the degradation of dG, indicating that PPRIs involved in indirect photodegradation play a major role in the degradation of dG. This may be related to the lower redox potential of dG (Neeley and Essigmann, 2006).

The degradation of dG dominates the photodegradation of Tc-ARG in the presence of DOM in surface water, of which direct photodegradation and oxidative photodegradation were quite different. According to previous studies, 8-oxo-dG is the main product of environmental degradation of DNA (Li et al., 2005; Cheng et al., 1992). Therefore, to prove the role of dG in e-ARGs degradation, the main oxidation products of dG were detected before and after 12 h light irradiation. It can be seen from Fig. S7 that the concentration of 8-oxo-dG in the plasmid pBR322 solution was 2.70 μg L^{-1} before illumination, and the concentration significantly increased to 13.46 and 39.28 μg L^{-1} in PBS and SRFA solution, respectively. This result indicates that the oxidation reaction initiated by the PPRIs could promote the conversion of dG to 8-oxo-dG. This is consistent with the results of a previous study on oxidative damage of DNA (Yoon et al., 2017). Based on the above results, it can be concluded that sunlight can induce the degradation of the four deoxynucleosides in Tc-ARG, and DOM promoted the oxidative degradation of deoxynucleosides, especially dG, by producing PPRIs.

3.4. Photodegradation of four DNA bases

DNA bases (G, C, A, and T) are usually considered to be the deep degradation products of DNA (Dizdaroglu and Jaruga, 2012). Thus, the photodegradation of the four DNA bases was explored, and the results showed that except for A, the other three bases could undergo direct photodegradation under simulated sunlight irradiation (Fig. 4). The k_{obs} values of G, T, and C were 0.176 ± 0.005, 0.033 ± 0.002, and 0.036 ± 0.001 h^{-1}, respectively.

In SRFA solutions, the photodegradation of G, T, and C was faster compared with the photodegradation rates in PBS with k_{obs} values of 0.342 ± 0.007, 0.062 ± 0.000, and 0.082 ± 0.005 h^{-1}, respectively. This finding highlights the promotional effect of SRFA on the degradation of the four bases. Among them, G was degraded fastest in the SRFA solution, which is in accordance with the degradation of dG during the photodegradation of Tc-ARG, in which SRFA significantly promoted its degradation. The reactivity of the four bases with $^1O_2$ and HO• was

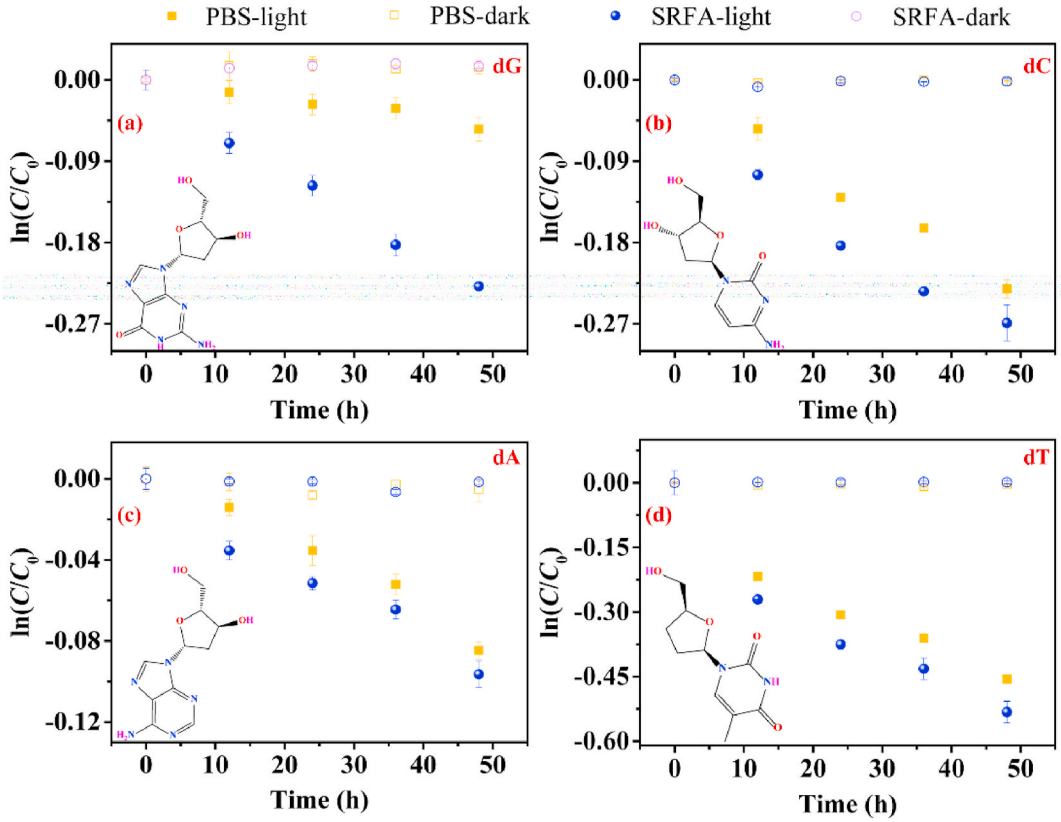

Fig. 3. Deoxynucleosides photodegradation in e-ARGs in PBS and SRFA solutions under simulated sunlight irradiation (pH = 7.0, C_0 = 10 μg mL^{-1}, SRFA: 10 mg L^{-1}).

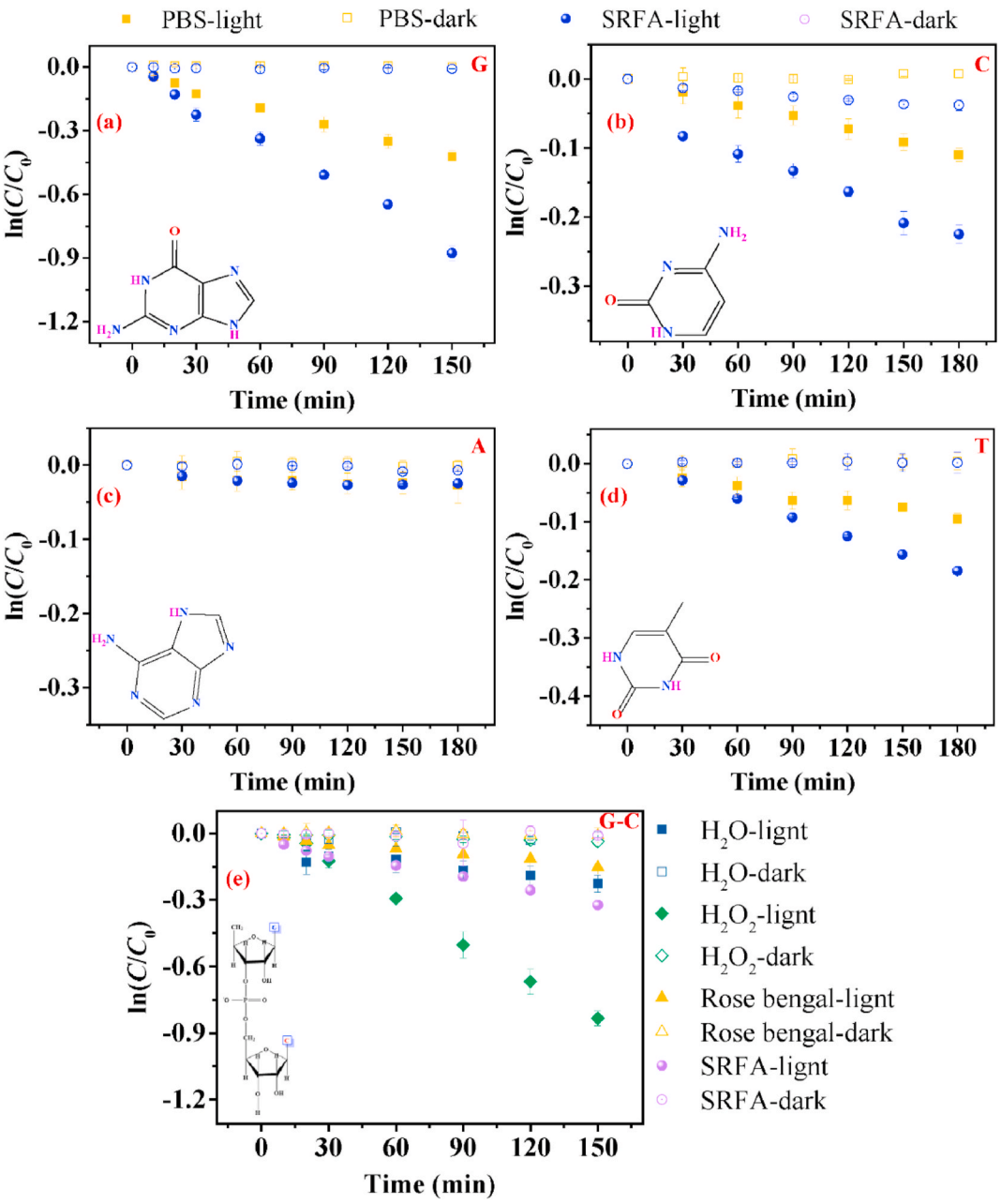

Fig. 4. Bases and double base photodegradation of DNA in different solutions under simulated sunlight irradiation (pH = 7.0, C_0 = 5 μg mL^{-1}).

determined in RB and H_2O_2 solutions to further investigate the photodegradation pathways (Fig. S9). The results showed that G and T can be oxidized by $^1O_2$ and all the four bases can be oxidized by HO• fastly. Thus, HO• may play an important role in the photodegradation of the four bases in e-ARGs in sunlit surface water.

All four deoxynucleosides could undergo direct photodegradation (Fig. 3), while the three single bases except G were degraded slowly (T and C) or basically not degraded (A) under direct irradiation (Fig. 4). This finding indicates that the deoxyribose group in the DNA can also undergo photodegradation and may contribute to the photodegradation of e-ARG. In the SRFA solution, the degradation rate of all deoxynucleosides and single bases could be significantly promoted due to the generation of PPRIs, and they could be quickly oxidized by HO• (Figs. 3 and 4). This also verified the important role of HO• in the degradation of e-ARGs.

The photodegradation behavior of double-based DNA (taking G-C as an example) was further studied for better understanding the photodegradation pathways of e-ARGs. G-C was selected due to the degradability of dG, dC, G, and C in both PBS and SRFA solutions under simulated sunlight irradiation. The result showed that G-C could be directly photodegraded with a value of k_{obs} of 0.101 ± 0.012 h^{-1} (Fig. 4 (e)). In SRFA solution, the value of k_{obs} of G-C increased to 0.133 ± 0.006 h^{-1}, indicating the promotional effect of SRFA on the photodegradation of G-C. Thus, the potential reactions of G-C induced by HO• and $^1O_2$ were investigated and the results showed that the yield of $^1O_2$ oxidative degradation of G-C was low as the k_{obs} values of G-C in solutions with RB (0.062 ± 0.003 h^{-1}) were lower as compared with the values in PBS. Similar to single bases, HO• induced oxidative degradation was also the main degradation pathway for double-based e-ARGs as the k_{obs} values of G-C in H_2O_2 solutions increased to 0.328 ± 0.009 h^{-1} (Table S6 in the SI). Therefore, in SRFA solutions, HO• may play a crucial role in the indirect photodegradation of G-C. In natural waters, multi-base DNA strands with bases as the basic unit could also undergo direct photolysis and indirect photolysis initiated by PPRIs from DOM.

3.5. Microscopic reaction pathways of e-ARGs with HO

The experimental results showed that the pBR322 plasmid-encoded Tc-ARG can undergo direct and indirect photodegradation in natural waters under simulated sunlight irradiation. Faster degradation of Tc-ARG in H_2O_2 solution compared with that in PBS was observed (Fig. 1), which indicated that the oxidation by HO• could accelerate the degradation of Tc-ARG, and HO• could play an important role in the degradation of specific bases (e.g. G). Besides, as reported in previous study, HO• could induce DNA strand breaks by extracting H from sugar fractions of DNA (Dizdaroglu, 2012). However, at present, the microscopic reaction pathways of e-ARGs with HO• are not yet clear. Thus, the reaction pathways of the four bases of Tc-ARG (G, C, A, and T) and a double-based DNA (G-C) with HO• were investigated using DFT calculation.

The reactions between chemical substances and HO• are mainly carried out through the addition of unsaturated compounds or through H-abstraction (Zhou et al., 2011). The four bases, G, C, A, and T have 6, 4, 8, and 2 addition positions and 5, 5, 5, and 6 H-abstraction positions, respectively (Fig. 5). The possible addition and H-abstraction pathways of the four bases reacting with HO• were calculated. The Gibbs free energy change (ΔG), the enthalpy change (ΔH), and the activation free energy ($\Delta G^{\ddagger}$) were calculated, as shown in Table S7 and Fig. S14.

It can be seen in Table S7 and Fig S14 that for G the addition reactions at the C2, C4, C6, and C9 sites are with a negative value of ΔG and ΔH. This indicates that HO• addition to the C atom of the unsaturated bond in G is thermodynamically spontaneous and exothermic. Among the reactions, the HO• addition on the C2 site is an energy-free reaction, so the HO• addition on C2 site is more favorable. This leads to the generation of hydroxylated intermediate. The H-abstraction reaction at the H13 site is thermodynamically spontaneous and exothermic, while the same reaction cannot proceed spontaneously at the H12 site.

For C, the addition reactions at C4 and C5 are thermodynamically spontaneous and exothermic, while the reaction at the C3 site is thermodynamically unspontaneous and exothermic. The HO• addition on C4 site is more favorable to occur due to its lower $\Delta G^{\ddagger}$, leading to the generation of the 5-hydroxycytosine intermediate according with experimental results (Evans et al., 2004). For the H-abstraction reactions, the ΔG and ΔH of the reactions at H9 and H12 sites are less than 0, indicating that these reactions are thermodynamically spontaneous and exothermic.

For A, the addition reactions at C2, C4, C6, C8, and C9 sites are associated with negative values of ΔG and ΔH, indicating that the HO• addition reaction is thermodynamically spontaneous and exothermic. Among the reactions, the HO• addition on the C2 site is an energy-free reaction, leading to the generation of the 8-hydroxyadenine intermediate, which is consistent with the findings reported in a previous study (Evans et al., 2004; Von Sonntag, 2006). For the H-abstraction reactions, the ΔG and ΔH of the reaction at the H11, H12, H13, and H15 sites are less than 0 and $\Delta G^{\ddagger}$ is less than 6.388 kcal mol^{-1}. This indicates that the reactions are thermodynamically spontaneous, exothermic, and can proceed spontaneously.

For T, the HO• addition on the C4 and C5 sites, and the H-abstraction reactions at the H15 site are energy-free reactions, showing that the reaction at these three sites is favorable to occur. This reaction generates hydroxyl addition intermediates (Evans et al., 2004). The H-abstraction reactions at the H11, H12, H13, and H14 sites are with ΔG and ΔH less than 0 and the $\Delta G^{\ddagger}$ is in all cases less than 5.791 kcal mol^{-1}. This means that these reactions can proceed spontaneously and exothermic, while the reaction at the H10 site is thermodynamically unspontaneous and endothermic.

Based on the results of the DFT calculations, the main reaction pathways of the four bases with HO• were proposed, as shown in Fig. 5. For the four bases, addition and H-abstraction reactions will occur in the presence of HO• in natural waters. This would lead to oxidative degradation of e-ARG, and subsequently inhibit its spread.

The 8-oxo-dG has been proven to be the main oxidation product of e-ARGs (Fig. S7). Therefore, the generation pathways of 8-oxo-dG from e-ARGs were investigated by calculating the reaction pathways of G-C (structures and atomic numberings of the base were shown in Fig. S15) with HO•. As can be seen in Fig. 6 and in Table S8 in the SI, G-C can react with HO• without an energy barrier to produce the intermediate (G-C + HO•) with a value of ΔG of −34.043 kcal mol^{-1} at the position C_2.

The intermediate (G-C + HO•) may undergo secondary reactions through 4 pathways: (1) It undergo a direct H-transfer reaction with $\Delta G^{\ddagger}$ of 53.789 kcal mol^{-1} and ΔG of 15.467 kcal mol^{-1}, leading to the generation of IM1. This reaction is unlikely to occur due to the high $\Delta G^{\ddagger}$ and positive ΔG; (2) H_2O catalyzed H-transfer with $\Delta G^{\ddagger}$ of 14.891 kcal mol^{-1} and ΔG of 5.885 kcal mol^{-1}, leading to the generation of IM2.

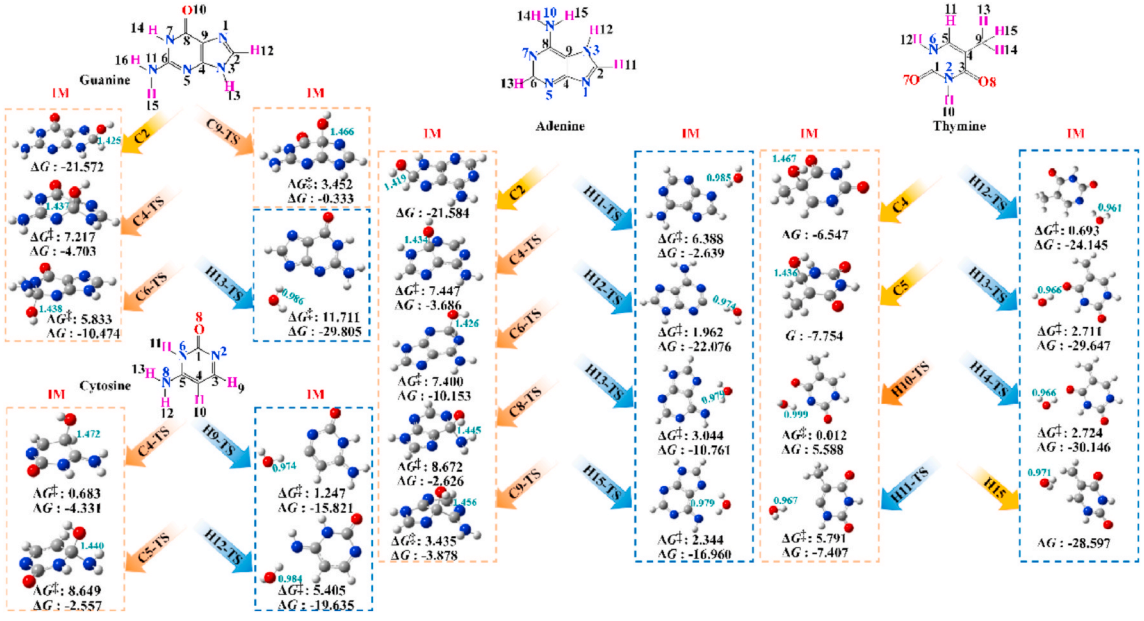

Fig. 5. Addition and H-abstraction reaction pathways of bases (G, C, A, T) with HO• ("IM" denote intermediate; and *Cm* and Hm for direct reaction with HO•, *Cm*-TS for HO• addition pathways, Hm-TS for H-abstraction pathways; the bonds unit is Å; the energy unit is kcal mol^{-1}).

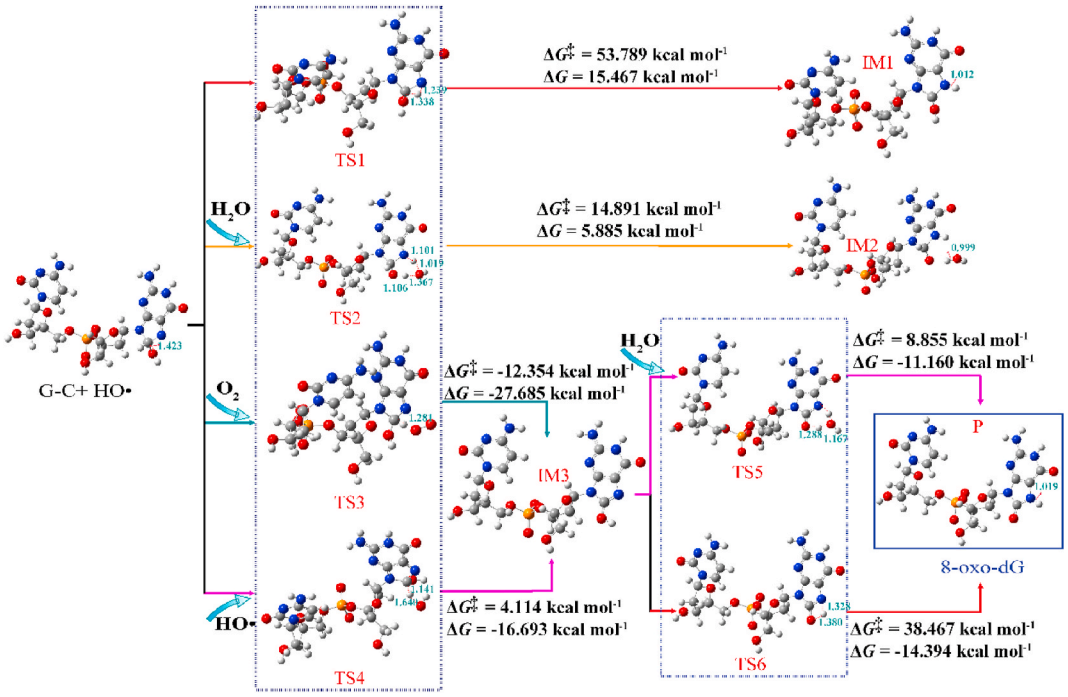

Fig. 6. Generation pathways of 8-oxo-dG in reaction of G-C with HO• ("IM" denotes intermediate; "TS" denotes transition states, "P" denotes the products formed; the values given are the length of the bonds marked with the red dashed lines, and the unit is Å). (For interpretation of the references to colour in this figure legend, the reader is referred to the Web version of this article.)

This pathway is dynamically possible but thermodynamically non-spontaneous; (3) Dissolved oxygen (O_2) initiated H-abstraction with $\Delta G^{\ddagger}$ of 12.354 kcal mol^{-1} and ΔG of −27.685 kcal mol^{-1}, leading to the generation of IM3. IM3 could undergo a H_2O catalyzed H-transfer reaction with $\Delta G^{\ddagger}$ of 8.855 kcal mol^{-1} and ΔG of −11.160 kcal mol^{-1}, leading to the generation of 8-oxo-dG. This pathway is dynamically and thermodynamically spontaneous. The IM3 could also undergo direct H-transfer to generate 8-oxo-dG with $\Delta G^{\ddagger}$ of 38.467 kcal mol^{-1} and ΔG of −14.394 kcal mol^{-1}. This pathway is unlikely to occur due to the high $\Delta G^{\ddagger}$. (4) Another HO• initiated H-abstraction reaction with $\Delta G^{\ddagger}$ of 4.114 kcal mol^{-1} and ΔG of −16.693 kcal mol^{-1}, which also leads to the generation of IM3. Although this pathway is dynamically and thermodynamically spontaneous, it is very difficult to occur as the concentration of HO• in natural waters is extremely low (10^{-18}-10^{-16} M) (Vione et al., 2006; McKay and Rosario-Ortiz, 2015).

The results provide above detail the pathways that are followed to generate 8-oxo-dG, one of the plasmid oxidation products, where two paths are more likely to occur. In the actual aquatic environment, due to the presence of DOM in water, HO• is produced under natural light irradiation, which induces oxidative degradation of e-ARGs, thereby blocking the spread of resistance.

3.6. Predicted photodegradation rate constant of Tc-ARG in estuary area

According to the research results, Tc-ARG can undergo direct photodegradation, and indirect photodegradation initiated by ^{3}SRFA*, $^1O_2$ and HO• generated by SRFA. Indirect photodegradation is more effective compared with direct photodegradation. Therefore, based on the steady-state concentration of PPRIs and the second-order reaction rate constants of Tc-ARG with these PPRIs, the overall photodegradation rate constant (k) of Tc-ARG as a function of water depth (z) and time (t) in the Yellow River estuary was predicted using the model established by Zhou et al. (2018). The results are shown in Fig. 7. For Tc-ARG, the maximum value of k in fresh water, estuary water, and sea water was calculated to be 0.524, 0.937, and 0.336 h^{-1}, respectively.

It can be seen in Fig. 7 that Tc-ARG was degraded fastest in estuarine water, as compared to fresh water and seawater. The photolysis half-life ($t_{1/2}$) of Tc-ARG was calculated to be 1.439, 0.708 and 1.208 d in fresh water, estuarine water and seawater, respectively, using the k values at a water depth of 2 m. For the estuary region, when going from river water to seawater, it was reported in a previous study that the DOM concentration in seawater is lower than the DOM level in freshwater[34]. Therefore, in the estuary area, the photolysis half-life of Tc-ARG will

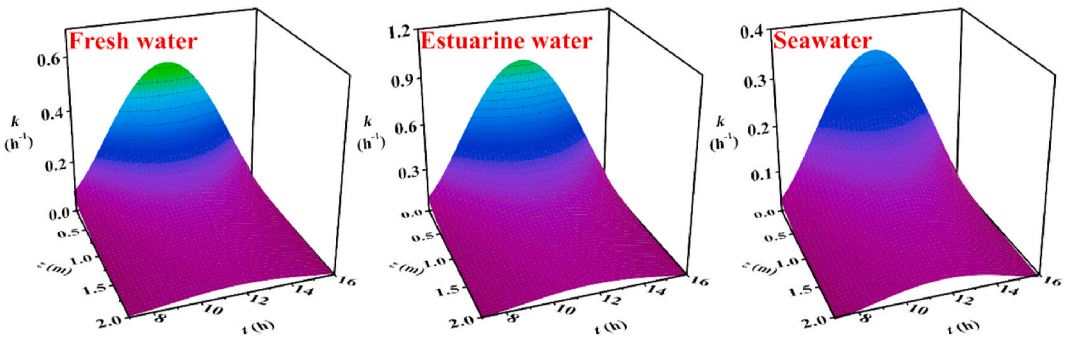

Fig. 7. Predicted photodegradation rate constants (k) of Tc-ARG in the fresh water, estuarine water and seawater at different water depths (z).

rapidly increase from river water to marine water, and its environmental persistence will gradually increase.

4. Conclusion

In this study, the photodegradation of cell-free Tc-ARG in water under sunlight irradiation was investigated. The results showed that Tc-ARG in the free state can be photochemically degraded under simulated sunlight irradiation, and its transformation could be inhibited due to the degradation of Tc-ARG. SRFA can promote the photodegradation of Tc-ARG due to the generated PPRIs, where the contribution rates of ^{3}SRFA*, $^1O_2$ and HO• were 39.76%, 0.21%, and 0.01%, respectively. The photodegradation of Tc-ARG is attributed to the degradation of deoxynucleosides, in which the deoxyribose group and the four bases (G, C, A, T) could be degraded under simulated sunlight irradiation. All the four bases can be oxidized by HO• through addition and H-abstraction reactions. The main oxidation product 8-oxo-dG was detected in the experiment and was proved to be generated through following pathways: HO• addition reaction on the C_2 site, dissolved oxygen initiated H-abstraction and followed by H_2O catalyzed H transfer reaction.

Based on the obtained photodegradation kinetic parameters, the photodegradation rate of Tc-ARG was predicted in the Yellow River estuary. The photolysis rates of Tc-ARG are very high and increased from river water to seawater, which will decrease its potential to spread in the natural waters. These results are indicative of the important role of sunlight irradiation in reducing the potential to spread of cell-free ARGs in the natural waters. Although ARGs could undergo fast photodegradation in surface waters under sunlight irradiation, they cannot be completely eliminated as the ARGs can be generated along with the proliferation of antibiotic resistant bacteria.

Author statement

Zhang Tingting: Conceptualization, Methodology, Software, Data curation, Writing – original draft preparation. **Cheng Fangyuan**: Software, Visualization, Investigation. **Yang Hao**: Data curation. **Zhu Boyi**: Software. **Li Chao**: Supervision. **Zhang Ya-nan**: Conceptualization, Supervision, Writing- Reviewing and Editing, Funding acquisition. **Qu Jiao**: Supervision, Project administration, Funding acquisition. **Willie J. G.M. Peijnenburg**: Writing- Reviewing and Editing.

Declaration of competing interest

The authors declare that they have no known competing financial interests or personal relationships that could have appeared to influence the work reported in this paper.

Acknowledgments

Funding information This research was funded by the National Natural Science Foundation of China [22176030, 42130705, 41877364, 21976027]; and by the Natural Science Foundation of Jilin Province [20200201049JC]; and by the "Thirteenth Five-Year" Science and Technology Research Planning Project of Jilin Provincial Department of Education [JJKH20200289KJ]; and by the Fundamental Research Funds for the Central Universities [2412020FZ015]; and also by the Jilin Province Science and Technology Development Projects [20210101110JC, 20200301012RQ, 20190303068SF].

Appendix A. Supplementary data

Supplementary data to this article can be found online at https://doi.org/10.1016/j.chemosphere.2022.134879.

References

Alekshun, M.N., Levy, S.B., 2007. Molecular mechanisms of antibacterial multidrug resistance. Cell 128 (6), 1037–1050.
Amarasiri, M., Sano, D., Suzuki, S., 2020. Understanding human health risks caused by antibiotic resistant bacteria (ARB) and antibiotic resistance genes (ARG) in water environments: current knowledge and questions to be answered. Crit. Rev. Environ. Sci. Technol. 50 (19), 2016–2059.
Bai, L., Jiang, Y., Xia, D., Wei, Z., Spinney, R., Dionysiou, D.D., Minakata, D., Xiao, R., Xie, H.-B., Chai, L., 2022. Mechanistic understanding of superoxide radical-mediated degradation of perfluorocarboxylic acids. Environ. Sci. Technol. 56 (1), 624–633.
Bellanger, X., Guilloteau, H., Bonot, S., Merlin, C., 2014. Demonstrating plasmid-based horizontal gene transfer in complex environmental matrices: a practical approach for a critical review. Sci. Total Environ. 493, 872–882.
Chang, P.H., Juhrend, B., Olson, T.M., Marrs, C.F., Wigginton, K.R., 2017. Degradation of extracellular antibiotic resistance genes with UV_{254} treatment. Environ. Sci. Technol. 51 (11), 6185–6192.
Chen, B.W., Liang, X.M., Nie, X.P., Huang, X.P., Zou, S.C., Li, X.D., 2015. The role of class I integrons in the dissemination of sulfonamide resistance genes in the Pearl River and Pearl River estuary, South China. J. Hazard Mater. 282, 61–67.
Chen, X., Yin, H., Li, G., Wang, W., Wong, P.K., Zhao, H., An, T., 2019. Antibiotic-resistance gene transfer in antibiotic-resistance bacteria under different light irradiation: implications from oxidative stress and gene expression Water. Res. 149, 282–291.
Cheng, C.F., Lin, H.H.-H., Tung, H.-H., Lin, A.Y.-C., 2022. Enhanced solar photodegradation of a plasmid-encoded extracellular antibiotic resistance gene in the presence of free chlorine. J. Environ. Chem. Eng. 10, 106984.
Cheng, K.C., Cahill, D.S., Kasai, H., Nishimura, S., Loeb, L.A., 1992. 8-hydroxyguanine, an abundant form of oxidative DNA damage, causes G-T and A-C substitutions. J. Biol. Chem. 267 (1), 166–172.
Chin, Y.-P., Miller, P.L., Zeng, L., Cawley, K., Weavers, L.K., 2004. Photosensitized degradation of bisphenol a by dissolved organic matter. Environ. Sci. Technol. 38 (22), 5888–5894.
Dang, B.J., Mao, D.Q., Xu, Y., Luo, Y., 2017. Conjugative multi-resistant plasmids in Haihe River and their impacts on the abundance and spatial distribution of antibiotic resistance genes. Water Res. 111, 81–91.
De Hoe, G.X., Zumstein, M.T., Getzinger, G.J., Rüegsegger, I., Kohler, H.-P.E., Maurer-Jones, M.A., Sander, M., Hillmyer, M.A., McNeill, K., 2019. Photochemical transformation of poly(butylene adipate-co-terephthalate) and its effects on enzymatic hydrolyzability. Environ. Sci. Technol. 53 (5), 2472–2481.
Dizdaroglu, M., Jaruga, P., 2012. Mechanisms of free radical-induced damage to DNA. Free Radic. Res. 46 (4), 382–419.
Dizdaroglu, M., 2012. Oxidatively induced DNA damage: mechanisms, repair and disease. Cancer Lett. 327, 26–47.
Edhlund, B.L., Arnold, W.A., McNeill, K., 2006. Aquatic photochemistry of nitrofuran antibiotics. Environ. Sci. Technol. 40 (17), 5422–5427.
Evans, M.D., Dizdaroglu, M., Cooke, M.S., 2004. Oxidative DNA damage and disease: induction, repair and significance. Mutat. Res./Rev. Mutat. 567 (1), 1–61.
Fan, J., Qin, H., Jiang, S., 2019. Mn-doped g-C_3N_4 composite to activate peroxymonosulfate for acetaminophen degradation: the role of superoxide anion and singlet oxygen. Chem. Eng. J. 359, 723–732.
Frisch, M.J., , T., G. W., Schlegel, H.B., Scuseria, G.E., Robb, M.A., Cheeseman, J.R., Scalmani, G., Barone, V., Petersson, G.A., Nakatsuji, H., Li, X., Caricato, M., Marenich, A.V., Bloino, J., Janesko, B.G., Gomperts, R., Mennucci, B., Hratchian, H. P., Ortiz, J.V., Izmaylov, A.F., Sonnenberg, J.L., Williams-Young, D., Ding, F., Lipparini, F., Egidi, F., Goings, J., Peng, B., Petrone, A., Henderson, T., Ranasinghe, D., Zakrzewski, V.G., Gao, J., Rega, N., Zheng, G., Liang, W., Hada, M., Ehara, M., Toyota, K., Fukuda, R., Hasegawa, J., Ishida, M., Nakajima, T., Honda, Y., Kitao, O., Nakai, H., Vreven, T., Throssell, K., Montgomery Jr., J.A., Peralta, J.E., Ogliaro, F., Bearpark, M.J., Heyd, J.J., Brothers, E.N., Kudin, K.N., Staroverov, V.N., Keith, T.A., Kobayashi, R., Normand, J., Raghavachari, K., Rendell, A.P., Burant, J. C., Iyengar, S.S., Tomasi, J., Cossi, M., Millam, J.M., Klene, M., Adamo, C., Cammi, R., Ochterski, J.W., Martin, R.L., Morokuma, K., Farkas, O., Foresman, J.B., Fox, D.J., 2016. Gaussian 16, Revision b.01. gaussian, inc., wallingford ct.
Fukui, K., 1981. The path of chemical reactions - the IRC approach. Acc. Chem. Res. 14 (12), 363–368.
Fu, Z., Wang, Y., Chen, J., Wang, Z., Wang, X., 2016. How PBDEs are transformed into dihydroxylated and dioxin metabolites catalyzed by the active center of cytochrome P450s: a DFT study. Environ. Sci. Technol. 50 (15), 8155–8163.
Grebel, J.E., Pignatello, J.J., Mitch, W.A., 2011. Sorbic acid as a quantitative probe for the formation, scavenging and steady-state concentrations of the triplet-excited state of organic compounds. Water Res. 45 (19), 6535–6544.
Guo, X., Jans, U., 2006. Kinetics and mechanism of the degradation of methyl parathion in aqueous hydrogen sulfide solution: investigation of natural organic matter effects. Environ. Sci. Technol. 40 (3), 900–906.
Jiang, L., Hu, X., Xu, T., Zhang, H., Sheng, D., Yin, D., 2013. Prevalence of antibiotic resistance genes and their relationship with antibiotics in the Huangpu River and the drinking water sources, Shanghai, China. Sci. Total Environ. 458–460, 267–272.
Latch, D., Stender, B., Packer, J., Arnold, W., McNeill, K., 2003. Photochemical fate of pharmaceuticals in the environment: cimetidine and ranitidine. Environ. Sci. Technol. 37 (15), 3342–3350.
Leresche, F., von Gunten, U., Canonica, S., 2016. Probing the photosensitizing and inhibitory effects of dissolved organic matter by using N,N-dimethyl-4-cyanoaniline (DMABN). Environ. Sci. Technol. 50 (20), 10997–11007.

Li, R., Zhao, C., Yao, B., Li, D., Yan, S., O'Shea, K.E., Song, W., 2016. Photochemical transformation of aminoglycoside antibiotics in simulated natural waters. Environ. Sci. Technol. 50 (6), 2921–2930.
Li, C., Xie, H.-B., Chen, J., Yang, X., Zhang, Y., Qiao, X., 2014. Predicting gaseous reaction rates of short chain chlorinated paraffins with •OH: overcoming the difficulty in experimental determination. Environ. Sci. Technol. 48 (23), 13808–13816.
Li, C.-S., Wu, K.-Y., Chang-Chien, G.-P., Chou, C.-C., 2005. Analysis of oxidative DNA damage 8-hydroxy-2'-deoxyguanosine as a biomarker of exposures to persistent pollutants for marine mammals. Environ. Sci. Technol. 39 (8), 2455–2460.
Luo, Y., Zhou, Q.X., 2008. Antibiotic resistance genes (ARGs) as emerging pollutants. Acta Sci. Circumstantiae 28 (8), 1499–1505.
Luo, Z., Spinney, R., Wei, Z., Hu, W.-P., Villamena, F.A., Song, W., Dionysiou, D.D., Xiao, R., 2021. Reevaluation of the reactivity of superoxide radicals with a sulfonamide antibiotic, sulfacetamide: an experimental and theoretical study. ACS ES&T Water 1 (11), 2339–2347.
McKay, G., Rosario-Ortiz, F.L., 2015. Temperature dependence of the photochemical formation of hydroxyl radical from dissolved organic matter. Environ. Sci. Technol. 49 (7), 4147–4154.
McKinney, C.W., Pruden, A., 2012. Ultraviolet disinfection of antibiotic resistant bacteria and their antibiotic resistance genes in water and wastewater. Environ. Sci. Technol. 46 (24), 13393–13400.
Moreira, N.F.F., Narciso-da-Rocha, C., Polo-López, M.I., Pastrana-Martínez, L.M., Faria, J.L., Manaia, C.M., Fernández-Ibáñez, P., Nunes, O.C., Silva, A.M.T., 2018. Solar treatment (H_2O_2, TiO_2-P25 and GO-TiO_2 photocatalysis, photo-fenton) of organic micropollutants, human pathogen indicators, antibiotic resistant bacteria and related genes in urban wastewater. Water Res. 135, 195–206.
Neeley, W.L., Essigmann, J.M., 2006. Mechanisms of formation, genotoxicity, and mutation of guanine oxidation products. Chem. Res. Toxicol. 19 (4), 491–505.
Phattarapattamawong, S., Chareewan, N., Polprasert, C., 2021. Comparative removal of two antibiotic resistant bacteria and genes by the simultaneous use of chlorine and UV irradiation (UV/chlorine): influence of free radicals on gene degradation. Sci. Total Environ. 755 (2), 142696.
Pruden, A., Pei, R.T., Storteboom, H., Carlson, K.H., 2006. Antibiotic resistance genes as emerging contaminants: studies in northern Colorado. Environ. Sci. Technol. 40 (23), 7445–7450.
Qiao, M., Ying, G.G., Singer, A.C., Zhu, Y.G., 2018. Review of antibiotic resistance in China and its environment. Environ. Int. 110, 160–172.
Ravanat, J.-L., Douki, T., Cadet, J., 2001. Direct and indirect effects of UV radiation on DNA and its components. J. Photochem. Photobiol., A 63, 88–102.
Sinha, R.P., Hader, D.P., 2002. UV-induced DNA damage and repair: a review. Photochem. Photobiol. Sci. 1 (4), 225–236.
Vione, D., Falletti, G., Maurino, V., Minero, C., Pelizzetti, E., Malandrino, M., Ajassa, R., Olariu, R.-I., Arsene, C., 2006. Sources and sinks of hydroxyl radicals upon irradiation of natural water samples. Environ. Sci. Technol. 40 (12), 3775–3781.
Von Sonntag, C., 2006. Free-radical-induced DNA Damage and its Repair: A Chemical Perspective. Springer. Formation of Reactive Free Radicals in an Aqueous Environment, Berlin/Heidelberg, Germany, pp. 7–46.
Wang, H., Wang, J., Li, S., Ding, G., Wang, K., Zhuang, T., Huang, X., Wang, X., 2020. Synergistic effect of UV/chlorine in bacterial inactivation, resistance gene removal, and gene conjugative transfer blocking. Water Res. 185, 116290.
Wang, J.L., Chen, X.Y., 2020. Removal of antibiotic resistance genes (ARGs) in various wastewater treatment processes: an overview. Crit. Rev. Environ. Sci. Technol. 52 (4), 571–630.
Wenk, J., von Gunten, U., Canonica, S., 2011. Effect of dissolved organic matter on the transformation of contaminants induced by excited triplet states and the hydroxyl radical. Environ. Sci. Technol. 45 (4), 1334–1340.
Yoon, Y., Chung, H.J., Di, D.Y.W., Dodd, M.C., Hur, H.G., Lee, Y., 2017. Inactivation efficiency of plasmid-encoded antibiotic resistance genes during water treatment with chlorine, UV, and UV/H_2O_2. Water Res. 123, 783–793.
Zhang, Y., Li, A., Dai, T., Li, F., Xie, H., Chen, L., Wen, D., 2018a. Cell-free DNA: a neglected source for antibiotic resistance genes spreading from WWTPs. Environ. Sci. Technol. 52 (1), 248–257.
Zhang, X., Li, J., Fan, W.Y., Yao, M.C., Yuan, L., Sheng, G.P., 2019a. Enhanced photodegradation of extracellular antibiotic resistance genes by dissolved organic matter photosensitization. Environ. Sci. Technol. 53 (18), 10732–10740.
Zhang, T.Y., Hu, Y.R., Jiang, L., Yao, S.J., Lin, K.F., Zhou, Y.B., Cui, C.Z., 2019b. Removal of antibiotic resistance genes and control of horizontal transfer risk by UV, chlorination and UV/chlorination treatments of drinking water. Chem. Eng. J. 358, 589–597.
Zhang, Y.-N., Zhang, T.T., Liu, H.Y., Qu, J., Li, C., Chen, J.W., Peijnenburg, W.J.G.M., 2020a. Simulated sunlight-induced inactivation of tetracycline resistant bacteria and effects of dissolved organic matter. Water Res. 185, 116241.
Zhang, Y., Chen, J.W., Zhou, C., Xie, Q., 2018b. Phototransformation of 2,3-dibromopropyl-2,4,6-tribromophenyl ether (DPTE) in natural waters: important roles of dissolved organic matter and chloride ion. Environ. Sci. Technol. 52 (18), 10490–10499.
Zhang, Y.Y., Moores, A., Liu, J.X., Ghoshal, S., 2019c. New insights into the degradation mechanism of perfluorooctanoic acid by persulfate from density functional theory and experimental data. Environ. Sci. Technol. 53 (15), 8672–8681.
Zhang, X., Li, J., Yao, M.-C., Fan, W.-Y., Yang, C.-W., Yuan, L., Sheng, G.-P., 2020b. Unrecognized contributions of dissolved organic matter inducing photodamages to the decay of extracellular DNA in waters. Environ. Sci. Technol. 54 (3), 1614–1622.
Zhao, R., Yu, K., Zhang, J., Zhang, G., Huang, J., Ma, L., Deng, C., Li, X., Li, B., 2020. Deciphering the mobility and bacterial hosts of antibiotic resistance genes under antibiotic selection pressure by metagenomic assembly and binning approaches. Water Res. 186, 116318.
Zhou, C.Z., Chen, J.W., Xie, H.J., Zhang, Y.N., Li, Y.J., Wang, Y., Xie, Q., Zhang, S.Y., 2018. Modeling photodegradation kinetics of organic micropollutants in water bodies: a case of the Yellow River estuary. J. Hazard Mater. 349, 60–67.
Zhou, J., Chen, J., Liang, C., Xie, Q., Wang, Y., Zhang, S., Qiao, X., Li, X., 2011. Quantum chemical investigation on the mechanism and kinetics of PBDE photooxidation by •OH: a case study for BDE-15. Environ. Sci. Technol. 45 (11), 4839–4845.